# Sputter deposition from a $Ti_2AlC$ target: Process characterization and conditions for growth of $Ti_2AlC$


Jenny Frodelius, Per Eklund, Manfred Beckers, Per Persson,
Hans Högberg and Lars Hultman





Original Publication:

Jenny Frodelius, Per Eklund, Manfred Beckers, Per Persson, Hans Högberg and Lars Hultman, Sputter deposition from a $Ti_2AlC$ target: Process characterization and conditions for growth of $Ti_2AlC$, 2010, THIN SOLID FILMS, (518), 6, 1621-1626.
http://dx.doi.org/10.1016/j.tsf.2009.11.059

# Sputter-deposition from a $Ti_2AlC$ target: process characterization and conditions for growth of $Ti_2AlC$

J. Frodelius[a]*, P. Eklund[a], M. Beckers[a], P.O.Å. Persson[a], H. Högberg[a,b], L. Hultman[a]

[a] *Thin Film Physics Division, Department of Physics, Chemistry and Biology (IFM), Linköping University, SE-581 83 Linköping, Sweden*
[b] *Impact Coatings AB, SE-582 16 Linköping, Sweden*

**Abstract**

Sputter deposition from a $Ti_2AlC$ target was found to yield Ti-Al-C films with a composition that deviates from the target composition of 2:1:1. For increasing substrate temperature from ambient to 1000 °C, the Al content decreased from 22 at% to 5 at%, due to re-evaporation. The C content in as-deposited films was equal to or higher than the Ti content. Mass spectrometry of the plasma revealed that the Ti and Al species were essentially thermalized, while a large fraction of C with energies >4 eV was detected. Co-sputtering with Ti yielded a film stoichiometry of 2:0.8:0.9 for Ti:Al:C, which enabled growth of $Ti_2AlC$. These results indicate that an additional Ti flux balances the excess C and therefore provides for more stoichiometric $Ti_2AlC$ synthesis conditions.

KEYWORDS: MAX phase, Titanium Carbide, Compound target, Physical Vapor Deposition, Mass Spectrometry, XRD, TEM

* Corresponding author. Tel.: +46 13 288 919; Fax: +46 13 288 918.
*E-mail address*: jenfr@ifm.liu.se (J. Frodelius)

## 1. Introduction

$Ti_2AlC$, discovered by Nowotny et al. [1], belongs to the $M_{n+1}AX_n$ phases (M – transition metal, A - group 13-14, and X - carbon or nitrogen, n is equal to 1, 2 or 3). These phases are generally known for exhibiting properties such as machinability, damage tolerance, and thermal-shock resistance [2,3,4,5]. For bulk material, $Ti_2AlC$, and the related MAX (short for $M_{n+1}AX_n$) phase $Ti_3AlC_2$, have attracted attention because of their stability at temperatures up to 1400 °C. This property stems from the formation of a protective $Al_2O_3$ layer, which has a thermal expansion coefficient comparable to that of the MAX phase itself [6,7]. Thus, $Ti_2AlC$ is of technological interest for thermal barrier coatings [8]. For thin film synthesis of MAX phases, magnetron sputtering has become a popular technique [9]. Wilhelmsson et al. [10] synthesized $Ti_2AlC$ and $Ti_3AlC_2$ thin films of high crystalline quality from three elemental targets (Ti, Al, and C). However, magnetron sputtering from only one compound target would simplify the deposition process and enable upscaling. $Ti_3SiC_2$ [11,12] and $Cr_2AlC$ [13] thin films have been synthesized by sputtering from MAX phase targets. For the Ti-Al-C system, Walter et al. [14] sputtered from a $Ti_2AlC$ compound target and showed that the Ti:Al:C 2:1:1 stoichiometry of the target is not sustained within the films. However, $Ti_2AlC$ could be synthesized by co-deposition of Ti.

Here, we investigate the conditions for thin film synthesis by magnetron sputtering from a $Ti_2AlC$ compound target. In contrast to Walter et al., we find an excess of C in all films, independent of substrate temperature, while the temperature is crucial for the Al

content of the films due to extensive evaporation of Al above 700 °C. Ti is added by co-sputtering to balance the excess of C, which yields growth of $Ti_2AlC$.

## 2. Experimental details

### *2.1 Plasma Characterization*

Characterization of the plasma during sputtering from a $Ti_2AlC$ *MAXTHAL 211*™ (Kanthal AB, Hallstahammar, Sweden) compound target (Ti:Al:C = 2.0 : 1.05 : 0.99, 0.8-1.6 wt% O) was performed with a Hiden Analytical Inc. PSM003 energy resolved mass spectrometer which consists of a Bessel box energy filter and quadropole mass filter with a subsequent photo multiplier detection setup. Due to technical limitations the mass spectrometer could not be mounted in the actual film deposition chamber (c.f., section 2.2), but instead the spectrometer was mounted in a comparable ultra high vacuum (UHV) system. Also, on-axis mounting was not possible due to technical and geometrical constraints so that it faced the magnetron from above in a 45° off-axis position at a distance of 14 cm, see Figure 1a. The resulting energy distribution within the plasma therefore is only considered qualitatively. The entrance orifice of the spectrometer was kept at floating potential and had a diameter of 300 μm. Previous to the experiments the detection system was tuned with respect to $Ar^{2+}$ ions. During all experiments, a circular $Ti_2AlC$ target of 5 cm diameter was used, sputtered in dc mode with target powers at 25, 50, 100, 150, and 200 W (hence a maximum power density of 10 W/cm²) at varying argon pressure of 2, 4, and 8 mTorr. In the following text we will write these pressure values in Pa instead as 0.25, 0.5, and 1 Pa, respectively.

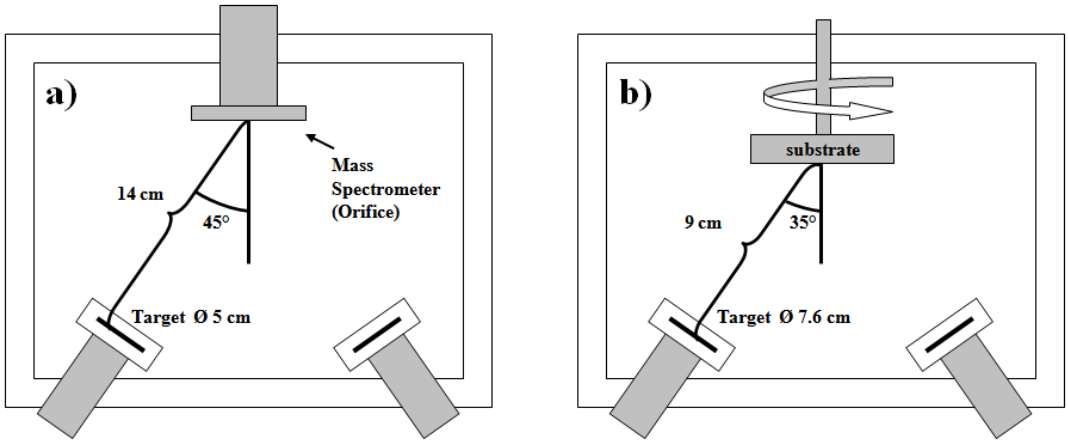


*Figure 1. Schematic of vacuum systems a) with mass spectrometer b) the deposition chamber.*

The plasma analysis consisted of a mass scan followed by ion energy distribution measurements of the elements detected. Note that during deposition mainly neutral atoms are sputtered, but the measurements were performed without secondary ionization, so only positive ions are detected. Ion masses were scanned from 0.4 to 100 atomic mass units (amu) in steps of 0.2 amu, with the exception of the point 40.0 amu to avoid saturation by $Ar^+$ ions. The energy distributions were measured from 0 to 10 V for Ti and Al and from 0 to 20 V for C. To rule out any deviation in plasma composition for different energies, a set of mass scans were performed at five different energies at 4, 8, 12, 16, and 20 eV. These experiments were carried out for the highest and lowest pressures of 2 and 8 mTorr, respectively. No difference was observed. Additional flat probe and Langmuir probe measurements were performed for both series of Ar pressure and target power to quantify the plasma potential.

*2.2 Thin Film Deposition*

Ti-Al-C thin films were deposited in a slightly different UHV chamber with a background pressure of $10^{-6}$ Pa. Here, the magnetrons faced the substrate holder from below in a 35° off-axis position with respect to the axis of sample rotation, see Fig. 1b. A circular $Ti_2AlC$ *MAXTHAL 211*™ and a pure metallic Ti target of 7.6 cm diameter each were used. The substrate holder was kept either at a distance of 9 cm to the targets and rotated at a speed of 23 rotations per minute, or at 6 cm, albeit without rotation due to geometrical restrictions. The substrate holder was kept at a floating potential of -10 V. The $Ti_2AlC$ and Ti targets were operated at a constant current of 400 mA, resulting in magnetron voltages around -365 V and -330V, hence a power density of ~3.2 W/cm², respectively. All depositions were carried out in Ar gas of purity 99.9999% at a pressure of 0.5 Pa (4 mTorr). $Al_2O_3$(0001) wafers of 10x10x1 mm³ size were used as substrates, which prior to deposition were cleaned ultrasonically in acetone and isopropanol, respectively, followed by in-situ heat treatment at the deposition temperature for one hour. The substrate temperature during deposition was varied from ambient to 1000 °C measured by thermocouple.

*2.3 Thin Film Characterization*

X-ray diffraction (XRD) θ-2θ scans were performed in an X-ray powder diffractometer (Philips PW 1729) with a line-focus $CuK_\alpha$ source operating at 40 mA and 40 kV. The diffraction patterns in Fig 4 and 5 have been smoothed using adjacent averaging. Pole figure measurements were performed in a Philips X'Pert MRD X-ray diffractometer

with a point focused $CuK_\alpha$ source operating at 40 mA and 45 kV. Elastic recoil detection analysis (ERDA) was performed with a 35 MeV $^{35}Cl^{7+}$ beam using a 5 MV tandem accelerator facility. The primary ions impinge onto the sample at an angle of 15° relative to the film surface. The energy and atomic number of the backscattered ions and the recoils are analyzed at a scattering angle of 30° in a Bragg ionization chamber filled with isobutane. An additional silicon detector was located at a scattering angle of 38° for hydrogen detection. Details of the overall experimental set-up can be found elsewhere [15]. The recoil energy spectra were transformed to elemental depth profiles using the ERDpro code, with an accuracy of around ±1 at%,

Bright-field transmission electron microscopy (TEM), high-resolution TEM (HREM) imaging and electron energy loss spectroscopy (EELS) were performed in a Tecnai $G^2$ F20U-Twin 200 kV field emission gun microscope. Cross-sectional specimens were mechanically polished to a thickness of ~50 μm, and subsequently thinned to electron transparency using a Gatan precision ion polishing system operated first at 5 kV using $Ar^+$ ions with a polishing step at 3 kV.

## 3. Results and discussion

### *3.1 Plasma Characterization*

Figure 2a shows a mass scan recorded during sputtering from the $Ti_2AlC$ at an Ar pressure of 0.5 Pa and a target power of 200 W. Clear peaks appear at atomic mass units of 12, 27, and 48, corresponding to C, Al, and Ti ions, respectively. The smaller peaks distributed on both sides of the Ti peak are due to different Ti isotopes. No compounds

of higher molecular weight, such as TiC, were detected. If clusters such as TiC were present, their energy would most likely correspond to the plasma potential. Therefore,

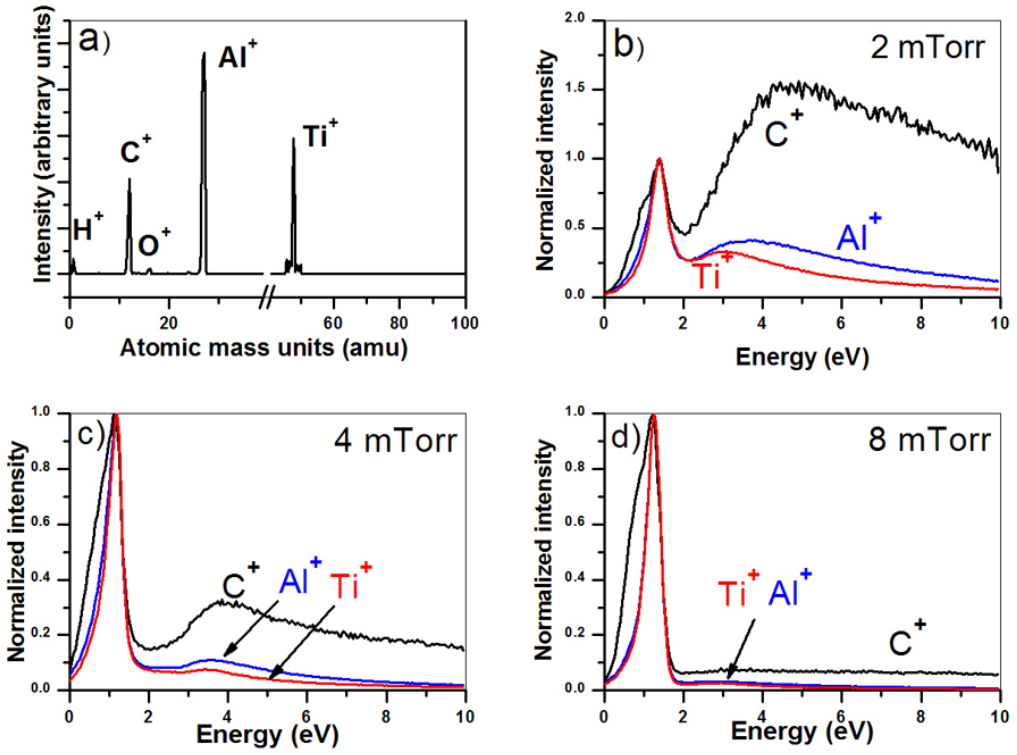


*Figure 2. a) Mass scan of plasma generated when sputtering from a $Ti_2AlC$ compound target at 200 W with Ar pressure of 0.5 Pa (no data was collected around 40 amu to avoid saturation of $Ar^+$ ions) and b)-d) energy distribution of Ti, Al and C ions in plasma when sputtered from a $Ti_2AlC$ target at 200 W with b) 0.25 Pa, c) 0.5 Pa, and d) 1.0 Pa. The mass scan was performed at an energy of 12 eV.*

an energy scan from 1 – 10 eV was performed at the mass of TiC, 60 a.m.u, but no TiC clusters were detected (no data shown). Measurements at Ar pressures of 0.25, 0.5, and 1.0 Pa and with target powers of 25, 50, 100, 150, and 200 W showed essentially the same result, i.e., no sputtered species other than Ti, Al, and C were detected.

Figure 2b, c, and d show the individual energy distribution of the Ti, Al, and C ions during sputtering at Ar pressures of 0.25, 0.5, and 1.0 Pa, respectively. All curves are normalized to the highest intensity. The peak between 1-2 eV in all spectra corresponds to the plasma potential as confirmed by Langmuir probe measurements (no data shown). At 1.0 Pa a major part of the Ti, Al, and C ions have an energy corresponding to the plasma potential. As the pressure decreases a larger fraction of ions with energy higher than the plasma potential is detected. This trend is more apparent for C, in particular at 0.25 Pa where a majority of the C ions exhibit higher energy with a broad distribution at >4 eV. This is explained by the thermalization distance for C, which at 0.25 Pa is longer than the target-to-substrate distance. Al and Ti also have a significant fraction of higher-energy ions at 0.25 Pa, but the peak at the plasma potential remains dominant. In order to relate the above results to the film growth experiments (section 3.2), we note that the conditions for sputtered particle thermalization at lower pressure are equivalent to its thermalization at a shorter target-to-substrate distance.

*3.2 Thin film deposition from a $Ti_2AlC$ target*

Figure 3 shows X-ray diffractograms of three thin films deposited from a $Ti_2AlC$ target at a target-substrate distance of 9 cm at substrate temperatures of 700, 850, and 1000 °C. The results show no $Ti_2AlC$ in any of the films. For the films deposited at 850 °C and 1000 °C, two sharp peaks are detected at 36.0° and 76.2°. The peak positions correspond to TiC 111 and 222. The peaks at 20.5° and 41.7° are the $Al_2O_3$ 0003 and 0006 substrate peaks, respectively. Pole figure measurements (not shown) confirm that the film deposited at 1000 °C and 850 °C have twinned grains due to

double domain nucleation areas of TiC {111} // $Al_2O_3$ {0001} (c.f. Ref. 16) with TiC <110> // $Al_2O_3$ <12;$\bar{1}$0>. The film deposited at 700 °C have shifted TiC 111 and 222 peak positions at 36.4° and 77.0°, respectively, with much lower intensity than for the films deposited at 850 °C and 1000 °C. This kind of disturbed crystal structure of TiC is most likely caused by growth of a (Ti,Al)C solid solution [17].

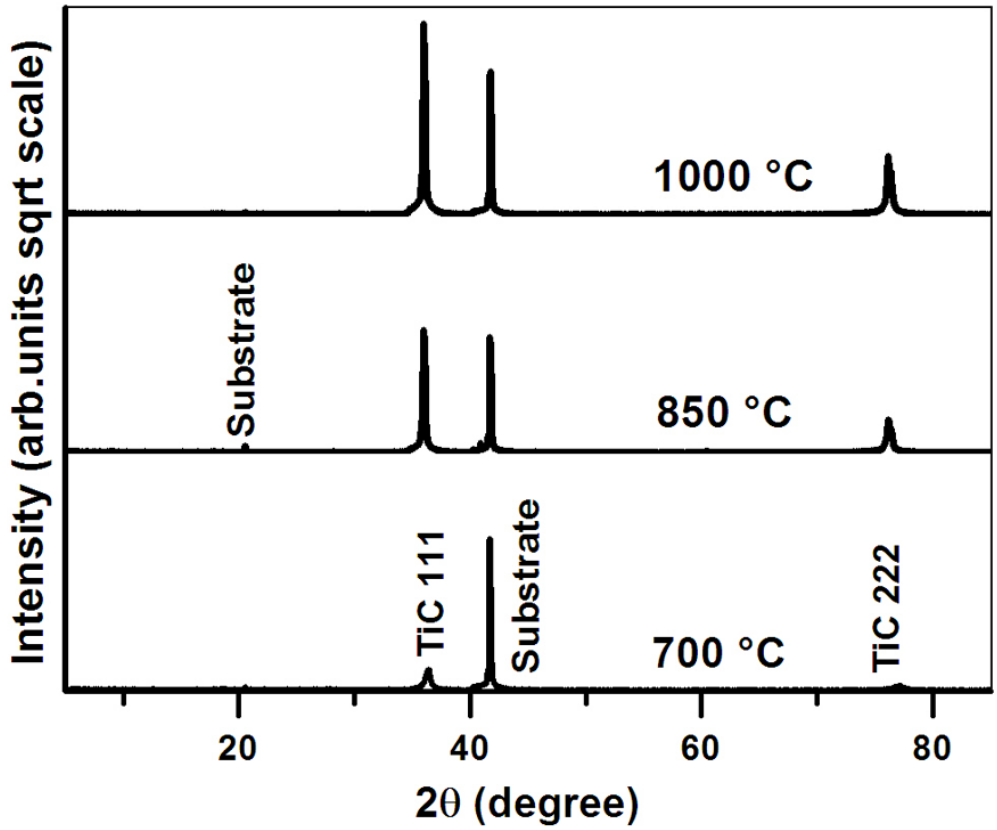


*Figure 3. X-ray diffractograms of films deposited from the $Ti_2AlC$ target at a target-to-substrate distance of 9 cm and substrate temperatures of 700 °C, 850 °C, and 1000 °C.*

Figure 4 shows x-ray diffractograms of films deposited at 1000 °C, 850 °C, and at ambient temperature at a target-to-substrate distance of 6 cm. The broad "peaks" around 9° and 19° were observed also in measurements on uncoated substrates and are most likely due to diffraction of bremsstrahlung from the highly crystalline substrate. The

peak at 40.3° originates from $L_\alpha$ of the W filament. Small amounts of the MAX phase $Ti_3AlC_2$ were obtained at 850 °C, as shown by the peaks at 2θ values of 9° and 39°. The films deposited at 850 °C and 1000 °C exhibits peaks from TiC 111. The TiC peak is clear at ambient temperature, although with a lower intensity than at 850 °C and 1000 °C. In comparison, epitaxial TiC has been synthesized from elemental sources at temperatures as low as 100 °C [18]. The Ti-Si-C system [19,20] also yields TiC at lower temperatures while the V-Ge-C [21] and Cr-Al-C [13] systems have been reported to yield X-ray amorphous films at 400 °C and 350 °C, respectively. The difference of MeC-forming temperatures between the systems is due to that the group-4 interstitial carbides (TiC, ZrC and HfC) are the most stable carbides of the transition metal carbides [22] and can therefore better withstand the disturbance from substitutional metal atoms such as Al.

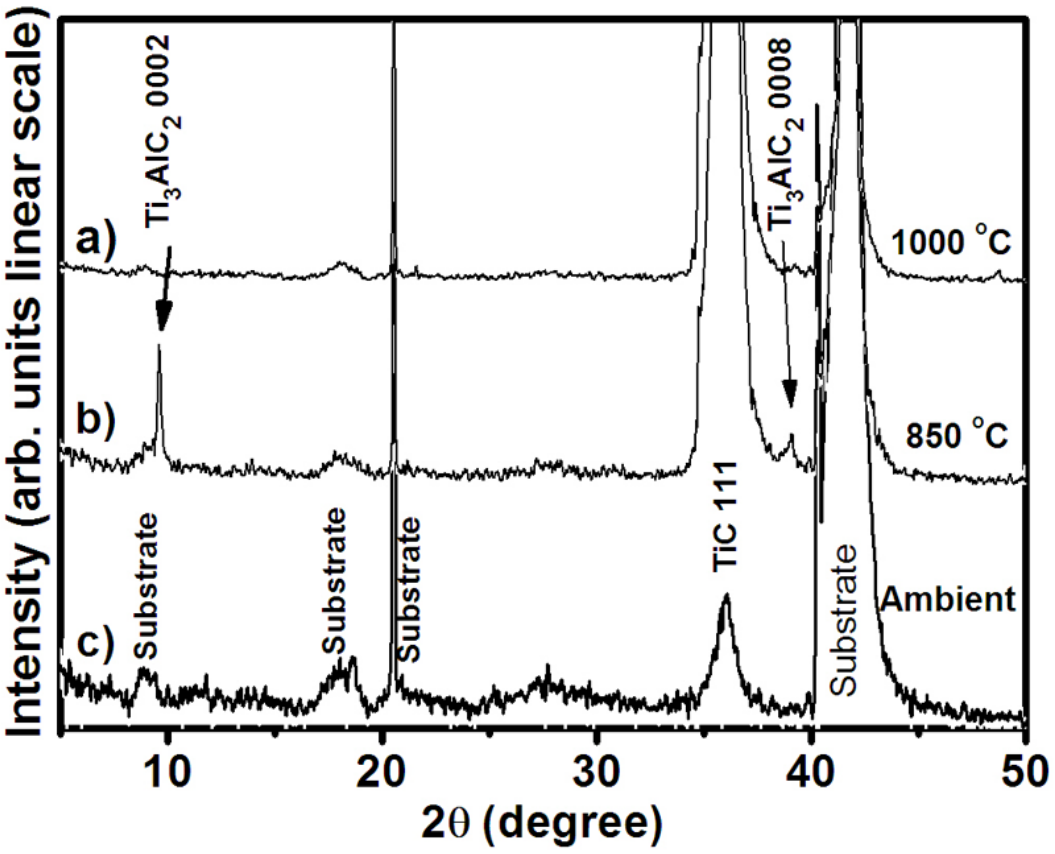

*Figure 4. X-ray diffractograms of films deposited from the $Ti_2AlC$ target at a target-to-substrate distance of 6 cm and substrate temperatures of ambient, 400 °C, 850 °C, and 1000 °C.*

Table 1 shows the composition of as-deposited films determined by ERDA. The impurity level of H and N is less than 2 at%. The nominal stoichiometry of $Ti_2AlC$ for Ti, Al, and C is 50, 25, and 25 at%, respectively. Irrespective of target-to-substrate distance, all films deposited at 700 °C or higher contain between 42 and 52 at% of C, which even exceeds the Ti content of 35 - 44 at%. We have seen the same excess of C when sputtering from a $Ti_3SiC_2$ compound target [12] and it was explained by the gas-phase scattering processes in combination with the angular and energy distribution of the sputtered species. This explanation is supported by Neidhardt et al. [23] who showed that when sputtering from Ti-B compound targets, the film composition is dependent on both the emission characteristics, and individual scattering processes. On the other hand the effect of bias, target constitution, and gas-type was reported to be moderate. However, the same arguments should apply to sputtering of, e.g., $Cr_2AlC$ compound target where stoichiometric 2:1:1 films have been synthesized [13]. It is known that $Ti_2AlC$ and $Cr_2AlC$ have different bonding character [24,25]. Therefore it is likely that the emission characteristics for, e.g., C vary depending on the MAX phase target. The difference in chemical activity between the species at the substrate surface could also be an important factor to obtain MAX phase films from compound targets.

In our work, besides the excess C, also the Al content decreases with increasing substrate temperature from 19 at% at 700 °C to less than 5 at% at 1000 °C. The as-deposited films at a distance of 6 cm had an Al content of 22 at% at ambient temperature. The strong temperature dependence of the Al content is not surprising

*Table 1. Composition analysis by ERDA of films deposited from the $Ti_2AlC$ target at substrate temperatures from ambient to 1000 °C and at a target-to-substrate distance of 6 cm and 9 cm. The level of N and H impurities are less than 2 at%.*

| Distance (cm) | Sub. Temp. (°C) | Ti | Al | C | O |
|---|---|---|---|---|---|
| | | (at %) | | | |
| 9 | 1000 | 41 | 3 | 52 | 2 |
| | 850 | 38 | 12 | 45 | 3 |
| | 700 | 35 | 19 | 42 | 3 |
| 6 | 1000 | 44 | 5 | 47 | 3 |
| | 850 | 40 | 9 | 44 | 4 |
| | Ambient | 35 | 22 | 37 | 4 |
| Co-sputtered | 700 | 51 | 19 | 23 | 7 |

given the high vapor pressure of metallic Al. Similar A-element deficiency has been reported for the Ti-Sn-C, V-Ge-C, and Ti-Si-C systems [26,17,12], where the evaporation tendency depends on the vapor pressure of each A-element. This shows the importance of the A-element properties for growth of MAX-phases. Nevertheless, epitaxial single-crystal $Ti_2AlN$ has been deposited by reactive magnetron sputtering at substrate temperatures as high as 1050 °C [27]. This result suggests that the limitation imposed by the high Al vapor pressure can be overcome by providing for more stoichiometric deposition conditions, which promote the bonding of the Al atoms to the $Ti_2N$ slabs of the MAX-phase. In the present work, the high carbon content of the as-deposited Ti-Al-C films may cause a hinder for Al to bond to Ti and instead form Al clusters that evaporate readily at temperatures around 700 °C.

The composition of films deposited at 850 °C (Figure 3b and Figure 4b) at target-to-substrate distances of 9 and 6 cm are similar (see Table 1). Despite the low Al content around 10 at% the MAX phase $Ti_3AlC_2$ is detected for the film deposited at 6 cm, but not at 9 cm. This suggests that the shorter distance leads to more sputtered species of

higher energy at the substrate, as discussed in section 3.1, which is beneficial for mobility during growth of the complex ternary structure of $Ti_3AlC_2$. The growth of $Ti_3AlC_2$ instead of $Ti_2AlC$ can be explained by the Al-poor and C-rich environment.

*3.3 Co-sputtering from a $Ti_2AlC$ and Ti target*

According to the ERDA analysis in Table 1, the as-deposited film sputtered solely from a $Ti_2AlC$ target at 700 °C and 9 cm has an Al content of 19 at%, but very high C content in relation to Ti. To balance this excess of C, Ti was added by co-sputtering with a Ti target. Figure 5 shows an X-ray diffractogram from a co-sputtered film at 700 °C where

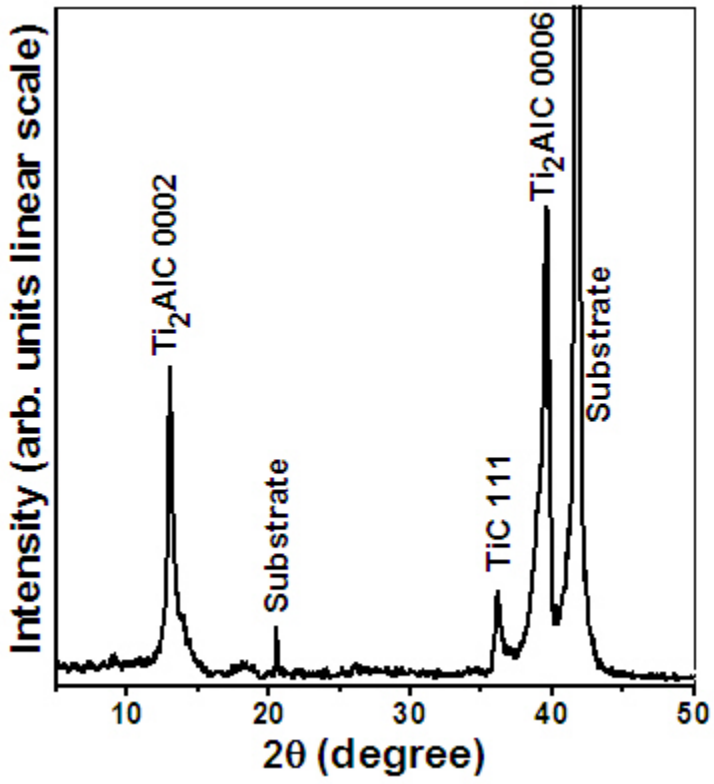


*Figure 5. X-ray diffractogram of film co-sputtered with $Ti_2AlC$ compound target and Ti target at 700 °C.*

two distinct peaks appear at 13.0° and 39.6°. These peaks originate from the (0002) and (0006) planes of $Ti_2AlC$. The TiC 111 peak is found at a 2θ value of 36.2° which corresponds to a smaller lattice parameter than for nearly stoichiometric TiC (35.9°) and therefore implies an understoichiometric $TiC_{1-x}$ and/or a substitution of Ti with Al [17,22]. ERDA (Table 1) showed that when adding Ti a composition of 51 at% Ti, 19 at% Al, and 23 at% C was obtained throughout the film which corresponds to a stoichiometry of 2:0.8:0.9. A surprisingly high oxygen content of 7 at% constant throughout the whole film was detected, despite the use of a UHV chamber. An EELS map over a $Ti_2AlC$ grain (not shown) shows that the oxygen is incorporated in the $Ti_2AlC$ structure. The effect of adding Ti during sputter deposition of MAX-phase films from a compound target has been reported for $Ti_2AlC$ [14] and for the Ti-Si-C system [12]. Walter et al. [14] show that Ti/Al ratio decrease with increasing temperature. Our results show the opposite, i.e., that there is a loss of Al not Ti at higher temperature, and it agrees well with what we reported for the Ti-Si-C system [12]. It is likely that Ti has the beneficial role of balancing the excess of C and thereby even out the competition between Al and C to bond to a Ti site. Thus, adding a Ti flux when sputtering from a $Ti_2AlC$ target provides for more stoichiometric $Ti_2AlC$ synthesis conditions.

Figures 6 a-c show TEM images of the film co-sputtered with Ti at 700 °C (cf. Figure 5). The microstructure of this film consists of grains up to ~0.5 μm long that extend throughout the film (Figure 6a). The magnified views of the $Ti_2AlC/Al_2O_3$ interface in Figure 6b and c recorded along the $Al_2O_3$ $<1\bar{1}00>$ zone axis demonstrate that the $Ti_2AlC$ grains grow with two out-of-plane orientations; $Ti_2AlC$ with basal planes perpendicular to the growth direction according to the experimental relationship $Ti_2AlC$

(0001) // $Al_2O_3$ (0001) and $Ti_2AlC$ with basal planes tilted for 37° of the growth direction, which implies the epitaxial relationship $Ti_2AlC$ (10$\bar{1}$7) // $Al_2O_3$ (0001).

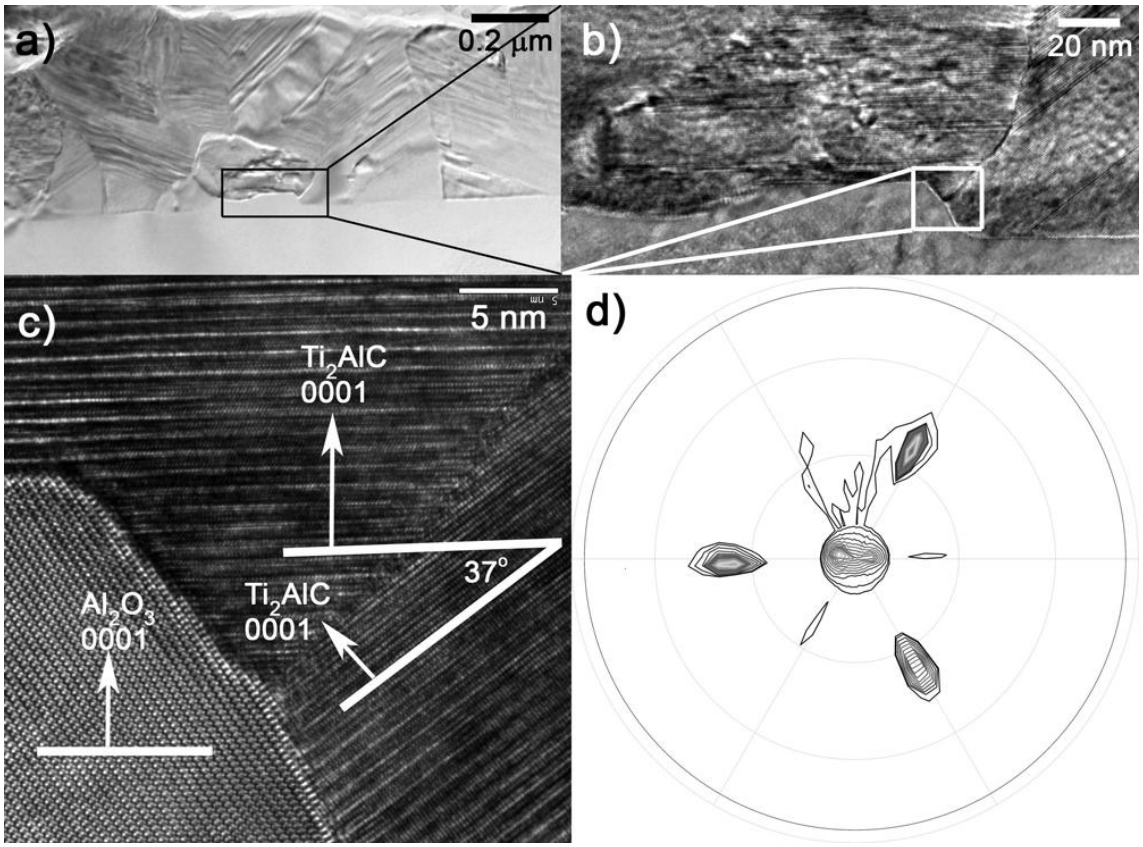


*Figure 6. Cross sectional TEM images from a film deposited by co-sputtering from $Ti_2AlC$ compound target and Ti target at 700 °C onto an $Al_2O_3$ (0001) substrate a) overview, b) magnified area from a), c) a HREM image of b) and, d) pole figure for the (0002) peak of $Ti_2AlC$.*

The inclined interface in Fig. 6c between the bottom $Ti_2AlC$ grain and $Al_2O_3$ has a local epitaxial relationship of (11$\bar{2}$2)//(11$\bar{2}$0) and [1$\bar{2}$10]//[1$\bar{1}$00].

Figure 6d is a pole figure of the 0002 peak of $Ti_2AlC$. The pole figure shows the epitaxial relationship of $Ti_2AlC$ (0001) // $Al_2O_3$ (0001) and a three-fold symmetry yielding an in-plane orientation relationship of $Ti_2AlC$ <$\bar{1}$2$\bar{1}$0> // $Al_2O_3$ <$\bar{1}$100> which

agrees with the above TEM results. The growth of the (000*l*) basal planes parallel to the $Al_2O_3$(0001) substrate is a common direction for epitaxial MAX-phase thin films, but it has also been reported that both $Ti_3SiC_2$ [16,28] and $Ti_2AlN$ [29] are able to grow in the <10$\bar{1}$*l*> directions on MgO (100) substrates. The uneven interface is due to a solid-state reaction between the film and substrate which provides for a source for both Al and O to be incorporated in the film [17,30]. Persson et al. showed that O can be substitutionally incorporated in C positions in the $Ti_2AlC$ structure [31].

## 4. Conclusions

We have shown how the composition of sputter-deposited Ti-Al-C films differs from the $Ti_2AlC$ compound target. The C content (42-52 at%) is higher than the Ti content (35-44 at%) for films deposited at 700, 800, and 1000 °C. It is shown that the energy distribution for C differs from Ti with a broad distribution at energies > 4eV. The difference in energy distribution together with difference in angular distribution during sputtering and scattering effects in the plasma causes a higher content of C in comparison to Ti. The Al content decreases substantially above 700 °C due to evaporation. The as-deposited films consist of TiC grown in preferred orientation of <111>. The sputtering process is stable when sputtered species of Ti, Al and C ions are present under a range of Ar pressure (0.25, 0.5, and 1.0 Pa) and target power (25, 50, 100, 150, and 200W). No other species from the sputtering process were detected. Addition of Ti by co-sputtering at 700 °C yielded a film stoichiometry of 2:0.8:0.9 for Ti:Al:C, which enabled the growth of $Ti_2AlC$ with a minority content of $TiC_x$. These results indicate that the addition of Ti suppresses the dominance of C and thereby a

more stoichiometric condition is provided for growth of $Ti_2AlC$. An additional Al content is also provided from the substrate through solid state reaction. The $Ti_2AlC$ has a preferred crystal orientation of (0001) // $Al_2O_3$ (0001) and $Ti_2AlC$ $(10\bar{1}7)$ // $Al_2O_3$ (0001).

**Acknowledgement**

The Swedish National Graduate School in Materials Science, the Swedish Research Council (VR), FunMat, and Kanthal AB are acknowledged for support. The ion beam analyses were performed at the Center for Application of Ion Beams to Materials Research under RITA Contract No. 025646.

**References**

[1] W. Jeitschko, H. Nowotny, Monatsh. Chem. **98** (1967) 328

[2] M. W. Barsoum, Prog. Solid State Chem. **28** (2000) 201

[3] J. Wang, Y. Zhou, Annu. Rev. Mater. Res **39** (2009) 415

[4] M. W. Barsoum, D. Brodkin, T. El-Raghy, Scr. Mater. **36** (1997) 535

[5] P. Eklund, M. Beckers, U. Jansson, H. Högberg, L.Hultman, Thin Solid Films, In press, 2009

[6] M. Sundberg, G. Malmqvist, A. Magnusson, T. El-Raghy, Ceram. Int. **30** (2004) 1899

[7] Z.J. Lin, M.J. Zhuo, Y.C. Zhou, M.S. Li, J.Y. Wang, Scr. Mater. **54** (2006) 1815

[8] R. Knight, M. W. Barsoum, United States Patent No. 0026845 A1, 4 Oct, 2001

[9] H. Högberg, L. Hultman, J. Emmerlich, T. Joelsson, P. Eklund, J.M. Molina-Aldareguia, J.-P. Palmquist, O. Wilhelmsson, U. Jansson, Surf. Coat. Technol. **193** (2005) 6

[10] O. Wilhelmsson, J.-P. Palmquist, T. Nyberg, U. Jansson, Appl. Phys. Lett. **85** (2004) 1066

[11] J-P Palmquist, U. Jansson, T. Seppänen, P.O.Å Persson, J. Birch, L. Hultman, P. Isberg, Appl. Phys. Lett. **81** (2002) 835

[12] P. Eklund, M. Beckers, J. Frodelius, H. Högberg, L. Hultman, J. Vac. Sci. Technol. A **25** (2007) 1381.

[13] C. Walter, D.P. Sigumonrong, T. El-Raghy, J.M. Schneider Thin Solid Films **515** (2006) 389.

[14] C. Walter, C. Martinez, T. El-Raghy, J. M. Schneider, Steel Res. Int. **76** (2005) 225 No 2/3.

[15] U. Kreissig, S. Grigull, K. Lange, P. Nitzsche, B. Schmidt, Nucl. Instrum. Methods Phys. Res., B **674** (1998) 136.

[16] J. Emmerlich, H. Högberg, S. Sasvári, P.O.Å. Persson, J.-P. Palmquist, U. Jansson, J.M. Molina-Aldarequia, Z. Czigány, L. Hultman, J. Appl. Phys. **96** (2004) 4817.

[17] O. Wilhelmsson, J.-P. Palmquist, E. Lewin, J. Emmerlich, P. Eklund, P.O.Å. Persson, H. Högberg, S. Li, R. Ahuja, O. Eriksson, L. Hultman, U. Jansson, J. Cryst. Growth **291** (2006) 290.

[18] H. Högberg, J. Birch, M.P. Johansson, L. Hultman, U. Jansson, J. Mater. Res. **16** (2001) 633.

[19] J.E. Krzanowski, S.H. Koutzaki, J. Am. Ceram. Soc. **84** (2001) 672.

[20] P. Eklund, J. Emmerlich, H. Högberg, O. Wilhelmsson, P. Isberg, J. Birch, P.O.Å Persson, U. Jansson, L. Hultman, J. Vac. Sci. Technol. B **23** (2005) 2486.

[21] O. Wilhelmsson, P. Eklund, H. Högberg, L. Hultman, U. Jansson, Acta Mater. **56** (2008) 2563.

[22] Handbook of Refractory Carbides and Nitrides, H.O. Pierson, Noyes Publications, Westwood, New Jersey, USA, 1996, ISBN: 0-8155-1392-5.

[23] J. Neidhardt, S. Mráz, J. M. Schneider, E. Strub, W. Bohne, B. Liedke, W. Möller, C. Mitterer, J. Appl. Phys **104** (2008) 063304.

[24] Z. Sun, D. Music, R. Ahuja, S. Li, J. M. Schneider, Phys. Rev. B **70** (2004) 092102

[25] D. Music, Z. Sun, A. Voevodin, J. M. Schneider, Solid State Commun. **139** (2006) 139.

[26] J. Emmerlich, P. Eklund, D. Rittrich, H. Högberg, L. Hultman, J. Mater. Res. **22** (2007) 2279.

[27] P.O.Å Persson, S. Kodambaka, I. Petrov, L. Hultman, Acta Mater. **55** (2007) 4401.

[28] P. Eklund, A. Murugaiah, J. Emmerlich, Zs. Czigàny, J. Frodelius, M.W. Barsoum, H. Högberg, L. Hultman, J. Cryst. Growth **304** (2007) 264.

[29] M. Beckers, N. Schell, R.M.S. Martins, A. Mücklich, W. Möller, J. Appl. Phys. **99** (2006) 034902.

[30] P.O.Å. Persson, J. Rosén, D.R. McKenzie, M.M.M. Bilek, C. Höglund, J. Appl. Phys. **103** (2008) 066102.

[31] P.O.Å. Persson, J. Rosén, D.R. McKenzie, M.M.M. Bilek, Phys. Rev. B, accepted 2009